NASA TECHNICAL NOTE

NASA TN D-1997

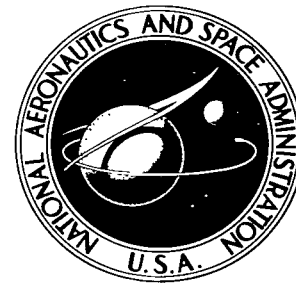

NASA TN D-1997

THE NATURE OF LIQUID FILM EVAPORATION DURING NUCLEATE BOILING

by Robert R. Sharp

Lewis Research Center
Cleveland, Ohio

NATIONAL AERONAUTICS AND SPACE ADMINISTRATION • WASHINGTON, D. C. • OCTOBER 1964

THE NATURE OF LIQUID FILM EVAPORATION DURING NUCLEATE BOILING

By Robert R. Sharp

Lewis Research Center
Cleveland, Ohio

NATIONAL AERONAUTICS AND SPACE ADMINISTRATION

For sale by the Office of Technical Services, Department of Commerce,
Washington, D.C. 20230 -- Price $0.75

THE NATURE OF LIQUID FILM EVAPORATION DURING NUCLEATE BOILING

by Robert R. Sharp

Lewis Research Center

SUMMARY

An evaporating liquid film formed at the base of bubbles during nucleate boiling was observed by two optical techniques. Interference of monochromatic light and reflection of polarized light yield film thickness against radius and time, local evaporative heat flux, and allow determination of wet and dry surfaces. The effects of different system parameters on bubble release, the evaporation process, and the boiling curve are discussed in relation to the experimental results.

INTRODUCTION

The observed high heat-transfer rates accompanying nucleate boiling has been attributed by some investigators to agitation associated with bubble formation and release. Recent investigations of temperature behavior on a boiling surface, however, have provided evidence that evaporation is the major heat-transfer mechanism in nucleate boiling regimes of relatively concentrated bubble populations. In reference 1, local surface temperature fluctuations during boiling were observed by noting the output of a high response thermocouple in conjunction with an oscilloscope. The temperature-time history was a series of rapid cooling periods of short duration followed by gradual reattainment of the initial temperature; the periodicity of the series was approximately that of the ebullition cycle. Transient heat fluxes during the cooling period were calculated to be about six times the gross value into the liquid. Time-temperature histories beneath large, discrete bubbles in low heat flux boiling were observed and the temperature data were matched with simultaneous high-speed motion pictures of the ebullition (ref. 2). In these experiments, a twentyfold surge in heat flux above the average occurred locally at the bubble base during the growth period; during bubble collapse, the heat flux fell to very low and even negative values. The extreme rapidity of cooling, and the fact that cooling took place inside the bubble base, demonstrated that evaporation must occur on or near the boiling surface. The temperature decrease appeared to be a continuous phenomenon lasting throughout the entire growth period. This observation supported the view proposed in reference 3

(p. 15, discussion by Snyder; p. 30, discussion by Bankoff) that evaporation occurs from a thin liquid film left by an expanding bubble at its base.

Evaporation from this liquid sublayer probably accounts for the major fraction of heat transfer in well-developed nucleate boiling regimes. The fraction of the heat flux transferred during the cooling period was calculated (ref. 1) by multiplying the heat removed per temperature drop by the cycle frequency; the data show that in the boiling of water on Nichrome at a heat flux of 135,000 and 202,000 Btu per hour per square foot, cooling at the bubble base accounts for well over half the total heat transfer. Experiments on condensation rates of steam bubbles also indicate that evaporation is of primary importance in the heat-transfer mechanism (ref. 4).

Although there is evidence that evaporation at the solid surface is the principal path of nucleate boiling heat transfer, no direct demonstration of a liquid microlayer has been made. There have, likewise, been no measurements of film thickness, which are essential in determining the maximum evaporative heat flux that can be transported through the bubble base. Whether the bubble base becomes completely dry, and if so, under what condition this occurs is of primary importance in understanding heat transfer to vapor columns and possibly burnout phenomenon as well. A hypothesis has also been advanced (ref. 5, p. 47) that "transition boiling is a combination of unstable film boiling and unstable nucleate boiling, each of which alternately exists at a given location on the heating surface." (Transition boiling here means the boiling regime for which heat flux decreases with increasing wall temperature.) This hypothesis, if true, indicates that properties of the microlayer may control the boiling curve in transition boiling. Finally, a study of the microlayer is necessary for a thorough understanding of the effects of surface material, surface thickness, additives, surface roughness, and so forth, on the boiling curve.

In this report, two experiments involving direct observations of the proposed microlayer are reported. The first (experiment A) was used to demonstrate the existence of a liquid film on polished glass surfaces and to investigate qualitatively the possibility of complete surface drying. The second (experiment B) was used to measure thickness profiles on the microlayer as a function of time and radius of the bubble base. From measurements of the thickness profiles, calculations can be made of local transient heat fluxes and evaporation rates. The results of these experiments and other pertinent boiling data have been used in an attempt to select those characteristics of the microlayer that markedly affect the nucleate boiling curve and to determine the relative importance of these characteristics with respect to system variables that specify bubble size, frequency, site population, and so forth.

SYMBOLS

A area

c constant

c_p	specific heat, cal/(g)(°C)
E_p	amplitude of perpendicularly polarized component of electric vector of reflected wave
E_s	amplitude of parallel polarized component of electric vector of reflected wave
F_p	perpendicular component of incident light wave
F_s	parallel component of incident light wave
H_{vap}	enthalpy per unit mass of vaporization, Btu/lb
k	thermal conductivity, cal/(cm)(°C)(sec)
l	positive integer
m	slope of thickness profiles
n	index of refraction
q	heat flux, Btu/(hr)(sq ft)
R	reflectance, percent
r	radius, in.
T_b	bulk liquid temperature
T_f	microlayer temperature
ΔT_{sat}	wall temperature minus saturation temperature
T_w	wall temperature
t	film thickness
V	volume, cu in.
α	thermal diffusivity, cm^2/sec
β	angle of incidence, deg
γ	angle of refraction, deg
λ	wavelength
ρ	density, g/cm^3
θ_β	Brewster's angle, deg

θ_γ angle of refraction in a thin film

τ time

APPARATUS AND PROCEDURE

Experiment A

The experiment described in this section was used to demonstrate, qualitatively, the presence of a microlayer during boiling. A liquid film can cause dramatic changes in the reflection properties of plane, polarized light from a transparent boiling surface. These changes are observed photographically and allow a simple basis for determining the wetting condition at the bubble base.

When unpolarized light is incident on any transparent interface, the light may be resolved into two plane polarized components, one perpendicular and one parallel to the plane of incidence. These two components reflect independently as described by Fresnel's equations for reflection of polarized light (see ref. 6, p. 39):

$$\frac{E_s}{F_s} = \frac{\tan(\beta - \gamma)}{\tan(\beta + \gamma)} \qquad \text{(parallel component)} \qquad (1a)$$

$$\frac{E_p}{F_p} = \frac{-\sin(\beta - \gamma)}{\sin(\beta + \gamma)} \qquad \text{(perpendicular component)} \qquad (1b)$$

where F_s and F_p are the respective values of the incident amplitudes. Equation (1b) shows that the reflected perpendicular component of the electric vector increases continuously, in absolute value, for all angles of incidence from 0° to 90°. The reflected parallel component, however, vanishes when the angle of incidence plus the angle of refraction equals 90°. This critical angle of incidence, for which the parallel component is 100 percent transmitted, is called Brewster's angle θ_β and depends only on the relative indices of refraction of the materials forming the interface for a given wavelength:

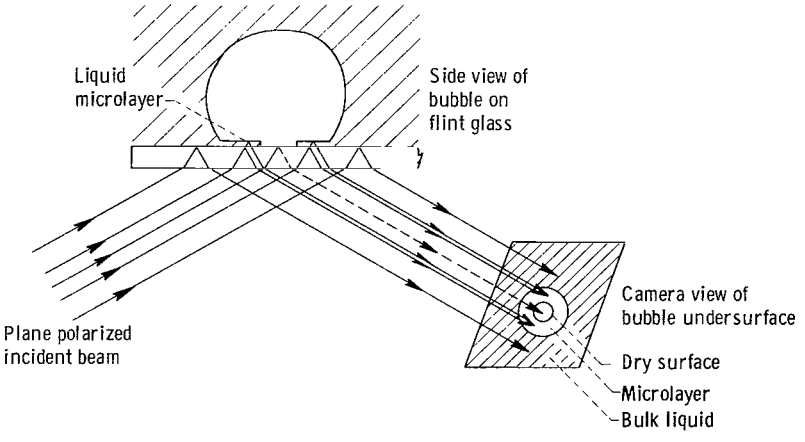

Figure 1. - Reflection of polarized light at bubble base in experiment A.

$$\tan \theta_\beta = \frac{n_2}{n_1} \qquad (2)$$

Experimentally, a collimated beam of mercury white light is directed onto a heated flint glass disk from be-

neath and reflected off the (upper) boiling surface (see fig. 1). The beam is incident at Brewster's angle for an air-flint glass boundary, with two polarizing filters oriented in the light path to block the perpendicular component. No appreciable light intensity is reflected from the lower glass surface, nor is light reflected from any dry region of the upper surface. When bulk liquid covers the glass, however, θ_β changes for the boiling surface, and a small percentage of light (0.354 percent) is reflected into the camera. (The percentage of reflection of the incident intensity can be calculated from eqs. (1a) and (2) and from the fact that the intensity is proportional to E_s^2, and from Snell's law. Reflectance values for interfaces in experiment A are shown in table I.) When a thin liquid film is present, reflection takes place off two interfaces, and the total intensity of reflected light is almost doubled (0.696 percent). All these calculations were made by using indices of refraction for the sodium D line. Multiple reflections within the glass disk will not occur because the reflected wave also meets the glass undersurface at θ_β and will thus be completely transmitted. Consequently, the base of a growing bubble should be sharply defined, so that the wetting condition will be immediately apparent by the relative intensities as shown in figure 1.

TABLE I. - PERCENTAGE REFLECTION OF PARALLEL POLARIZED COMPONENT FROM BOUNDARIES FORMED IN EXPERIMENT A

[Reflectances calculated from eq. (1a) by using indices of refraction at $\lambda = 5893$; β is calculated from Snell's law; θ_β is calculated from eq. (2).]

Interface	Angle of incidence, β, deg	Brewster's angle, θ_β, deg	Reflectance, R, percent
Flint glass - water	30.5	38.2	0.354
Flint glass - vapor	30.5	30.5	.000
Water - water vapor	40.4	37.0	.342
Flint glass - methanol	30.5	38.2	.354
Methanol - vapor	40.4	37.0	.342

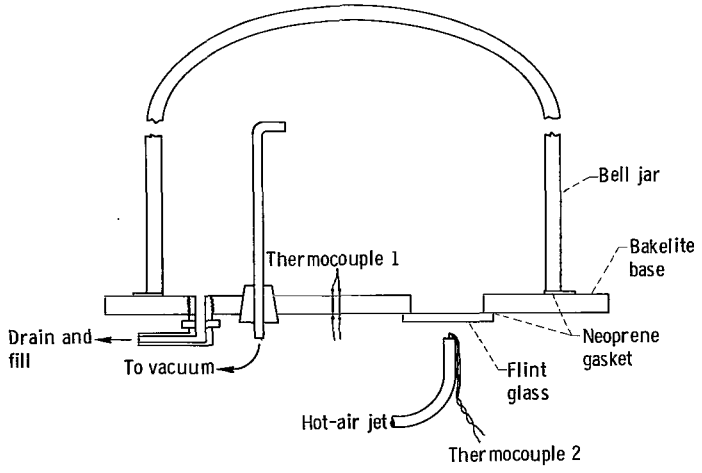

Figure 2. - Boiling apparatus for experiment A.

The boiling apparatus is shown in figure 2. Distilled, degassed water and methanol were boiled in a bell jar set on a Bakelite base. Connections for vacuum, fill and drain lines, and for a thermocouple to measure bulk temperature were fitted into the base. The glass disk ($2\frac{1}{4}$ in. diam. by $\frac{1}{8}$ in. thick) was placed beneath a 1-inch-diameter hole in the Bakelite base and was sealed for low pressures by a neoprene gasket. The glass disk contained a small scratch to facilitate nucleation. A perpendicular

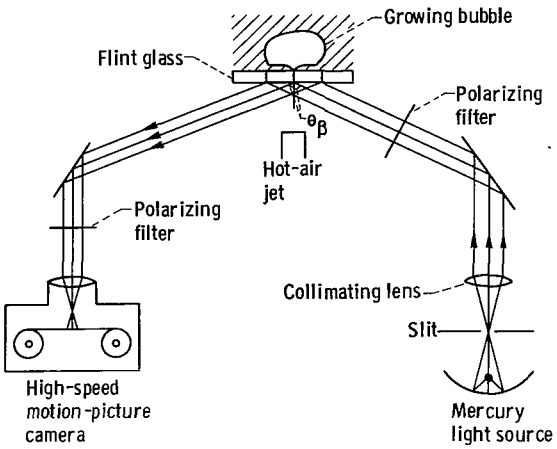

Figure 3. - Optical plan for experiment A. Polarized light incident at Brewster's angle, θ_β.

hot-air jet, 1/4 inch in diameter under 40 pounds per square inch gage was used for heating. To obtain the jet temperature, a 36-gage copper-constantan thermocouple was placed just inside the orifice. Unfortunately, gross heat fluxes in this system are difficult to calculate with any degree of accuracy.

The optical system, shown in figure 3, consisted of a high-voltage mercury light source, a slit, a collimating lens, a front-silvered mirror for adjusting the angle of incidence of the beam, and a second front-silvered mirror for directing the reflected beam into the high-speed motion picture camera through two polarizing filters. The polarizing filters were adjusted so that the dry flint glass surface reflected almost no light, but so that a drop of water on the upper surface was relatively bright and sharply defined.

Photographic interpretation in this experiment is simple and qualitative in nature. The expanding bubble base is easily distinguishable, and if a region of the base is uniformly brighter than the bulk liquid, the increased intensity must be due to a second interface immediately above the boiling surface. A dry surface will be darker than the bulk liquid.

Experiment B

Experiment A is a clear-cut method for determining whether a microlayer exists at the bubble base. If a microlayer is found, much more detailed evidence concerning the dimensions of the layer can be obtained from the interference phenomenon observed during the reflection of light off thin films. When monochromatic light is incident on a transparent thin film (the thickness must be the order of magnitude of wavelengths of light) reflection will take place off the upper and lower surfaces of the film. The reflected beam is a superposition of the reflected components, and since light can act as a wave phenomenon, these two components will interfere. Considering that $n_{\text{water vapor}} < n_{\text{water}} < n_{\text{flint glass}}$, constructive interference (addition of the reflected beams) will occur when the optical path length difference of these two components is an integral multiple of the wavelength. Destructive interference, reducing the initial intensity, will occur when the optical path length difference of these two components is an odd integral multiple of $\lambda/2$. If the angle of refraction through the film is θ_γ, the film thickness is t, the wavelength of light is λ, the refractive index of the liquid is n, and l is a positive integer or zero, intensity maximums of reflected light will occur when

$$t = \frac{l\lambda}{2n \cos \theta_\gamma} \tag{3a}$$

and intensity minimums when

$$t = \frac{(2l + 1)\lambda}{4n \cos \theta_r} \tag{3b}$$

as described in reference 7 (p. 367). A phase change of 180° is assumed at the second interface ($n_1 < n_2 > n_3$); in the case of the microlayer, this phase change does not occur ($n_1 < n_2 < n_3$). Hence, the referenced equations for minimums and maximums have been interchanged. The interference phenomenon is explained in detail in reference 6.

The postulated liquid film is assumed to be radially symmetric and of increasing thickness from the center to the edge, since the perimeter of the layer will have undergone the least evaporation. The resulting interference pattern should be a series of concentric light and dark rings, where each ring corresponds to a film thickness t, given by equation (3a) for the light rings and (3b) for the dark rings; l increases integrally from the center to the edge. A reference ring must, of course, be found to give absolute thickness, and methods for doing this are discussed in the section RESULTS. An interference pattern measures film thickness as a function of time and pattern radius. From this information, the rate of vapor evolution and the evaporative heat flux can be obtained.

Contrary to the method of experiment A, the beam of incident light is directed through the top of the bubble, and reflected off the microlayer back up through the top of the bubble (see fig. 4(a)). Only large discrete bubbles could be studied. As the bubble grows, the top bubble wall is flattened on a plastic window. A collimated beam of monochromatic light is directed by an adjustable mirror onto the boiling surface, and the reflected beam is recorded photographically by a high-speed camera.

The optical system consists of a mercury arc light source, a slit, a

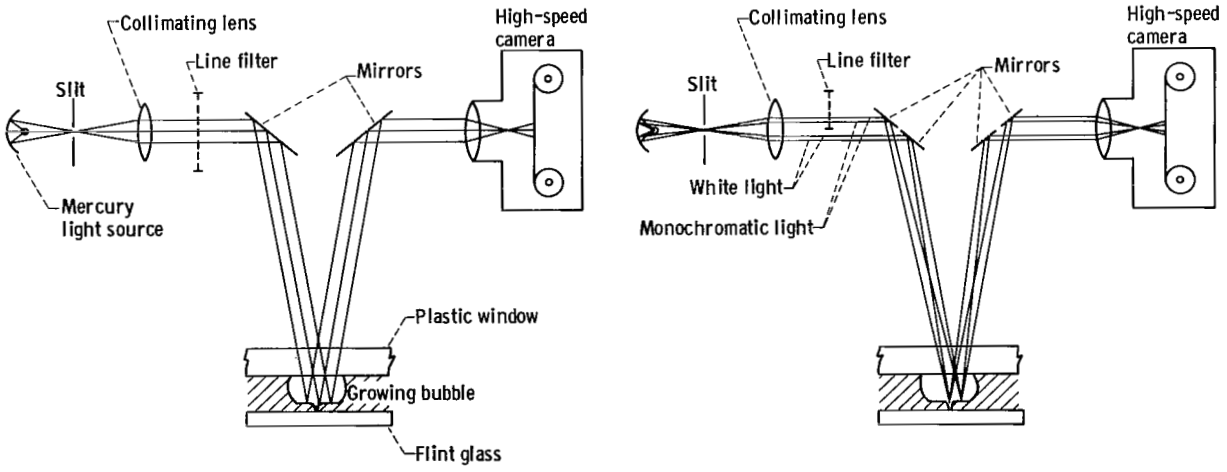

Figure 4. - Optical system for experiment B.

collimating lens, a line filter, adjustable mirrors, and a high-speed camera. The green line (5461 A) of mercury was selected by the line filter to obtain monochromatic light. For control experiments, a double-beam optical system was used in which the collimated beam was divided by a double-mirror system; one-half the beam was monochromatic (by use of line filter) and the other half was mercury white light (fig. 4(b)).

The percentage of incident light reflected from either interface of the film can be calculated from the equation

$$R = \left(\frac{n_2 - n_1}{n_2 + n_1}\right)^2 \tag{4}$$

by assuming normal incidence (ref. 7, p. 288). The actual angle of incidence is about 13° from the normal, a negligible correction for equation (4) since the $\tan^2$ of 13° is approximately equal to the sin of 13° (ref. 8, p. 511), but significant in calculating film thicknesses from equations (3a) and (3b). For a thin water film on the flint glass surface (n = 1.69) used, R equals 1.47 percent for the solid-liquid boundary and 1.90 percent for the liquid-vapor boundary. Concerning the relative contrast of light and dark rings, it should be noted that intensity minimums will be 0.540 percent of intensity maximums (see ref. 6, p. 63). The contrast rapidly decreases as the refractive index of the solid is lowered.

The boiling tank is shown schematically in figure 5. A flint glass disk D is mounted horizontally on a Bakelite support G, sealed with a neoprene gasket E, and held in place by three springs F. The glass boiling surface and the heating jet J are mounted in the tank on a threaded tubular assembly I, which allows adjustment of the distance between the boiling surface and the plastic window B. An auxiliary heater is used to obtain the desired pool temperature. Bulk pressure was lowered to approximately 0.1 atmosphere and the liquid temperature maintained at about 85° F. Reduced pressures had to be used to obtain bubbles large enough to study and obtain boiling with minimal thermal shock to the flint glass, which has a high coefficient of thermal expansion compared with other types of glass. The distance between the glass disk and plastic window was varied between 0.15 and 0.28 inch; of course, maximum bubble diameters were a good deal larger, usually between one-half and three-quarters of an inch. (This diameter refers to bubbles flattened

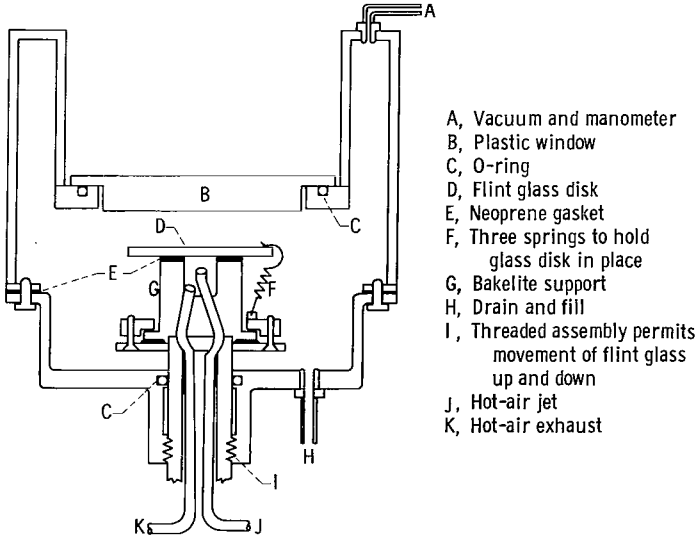

Figure 5. - Stainless-steel boiling tank for experiment B.

by the plastic window, and not bubbles growing freely in a pool.) A jet of hot (550° to 700° F) 40-pound service air provided the heating.

RESULTS

Experiment A

Surface film interference fringes. - Runs of boiling water and methanol on polished flint glass were made in experiment A. As explained previously, a liquid film at the bubble base will appear as a bright oval area on a field about half of that intensity. (The bubble base appears oval because the camera view is at Brewster's angle, or approximately 58° from the normal.) Complete drying of the film will be seen as a dark spot in the center of the bubble base. Sample pictures with the expected pattern are shown in figure 6 for methanol and in figure 7 for water. The black mark in the center of the frame is a scratch used for nucleation.

Figure 6 shows the base of a methanol bubble. A continuous surface film is indicated from the uniform and relatively highly reflected intensity at the base. A dark central region denoting surface dryness was not apparent for methanol or for water at the lower heat flux (fig. 7(a)). Drying at the base of water bubbles becomes evident (figs. 7(b) and (c)) as the heat flux increases. Often in the reflected patterns, curved dark fringes could be seen in the microlayer (see fig. 7(b)). These fringes are expected from the discontinuous nature of mercury white light, and their intensity and position are discussed in appendix A. A dry surface is relatively dark and appears as an expanding spot in the center of the bubble base. Interference fringes could be distinguished from dry surface both by their greater intensity and by the fact that fringes disappear more readily during bubble release than does a dry surface. The microlayer behavior during bubble release is discussed below.

The photographs in figure 7 were taken during one run of constant pressure and increasing heat flux. Unfortunately, the experimental setup made it difficult to obtain even approximate absolute values of heat flux; however, relative variations in the heat flux were easily observable from the gas jet temperature, and as long as half an hour was allowed for adjustment of the temperature gradient in the glass disk. The figure labels low heat flux for figure 7(a) and high heat flux for figures 7(b) and (c) are, therefore, only relative terms. The jet temperature increased about 100° F between low and high heat flux sequences. Surface drying was not shown to occur in figure 7(a) throughout the bubble life of 30.8 milliseconds. Two other low heat flux bubbles of the same run (not shown) likewise did not develop dry spots. At a higher heat flux, figures 7(b) and (c), a dry spot appears after 10 milliseconds regardless of maximum bubble diameter. In other high heat flux sequences, drying occurred between 5 and 10 milliseconds except for one small bubble, which remained wetted until release at 22.2 milliseconds. Clearly, the tendency for complete evaporation at the bubble base varies with heat flux. Since even the high heat flux sequences were discrete bubbles, it is interesting to note that appreciable drying can occur during slow boiling. The degree of drying probably depends chiefly on T_w at the time of nucleation; T_w determines the initial

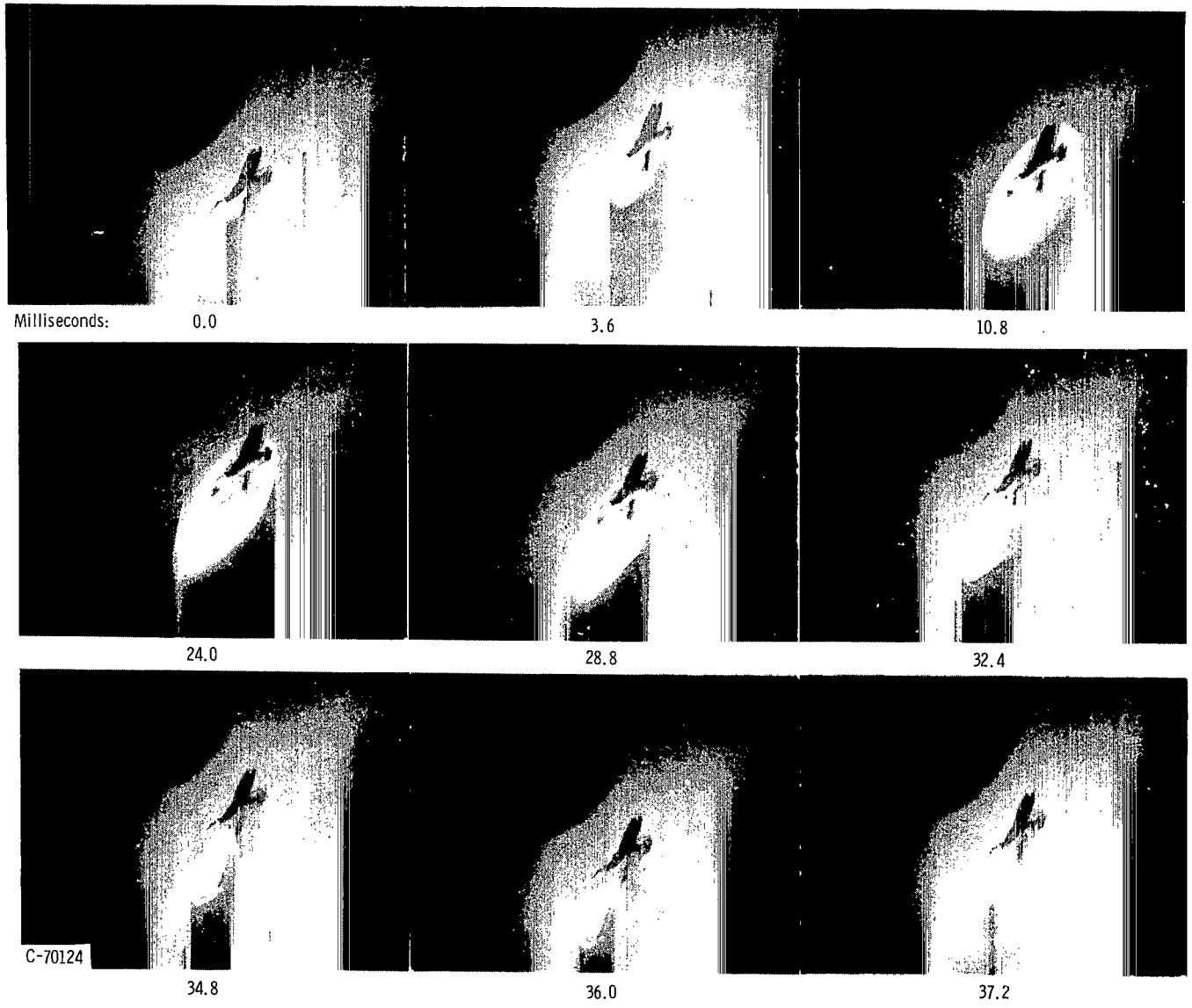

Figure 6. - Observation of microlayer: methanol boiling on flint glass.

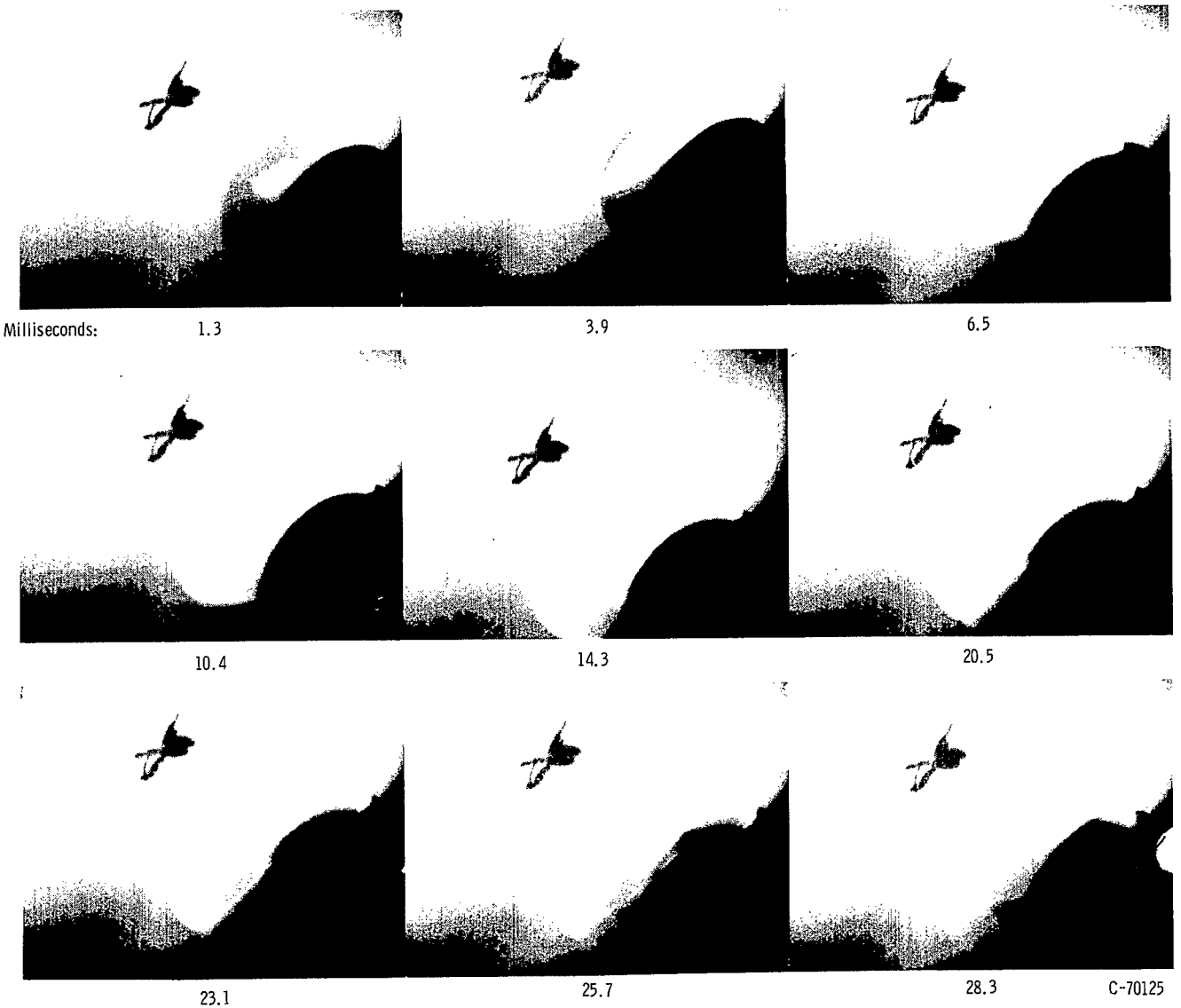

(a) Low heat flux.

Figure 7. - Observation of microlayer: water boiling on flint glass.

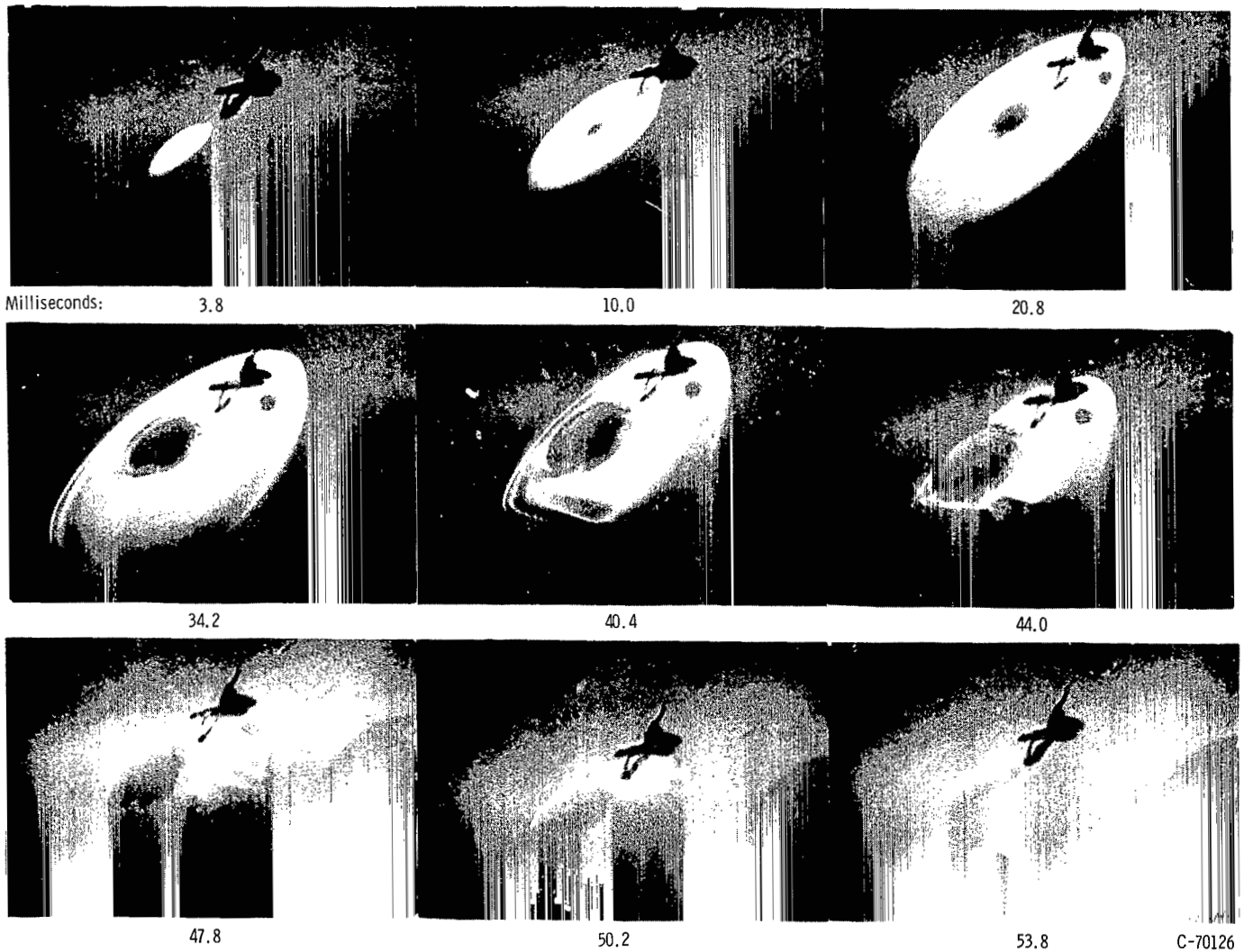

(b) High heat flux.

Figure 7. - Continued. Observation of microlayer: water boiling on flint glass.

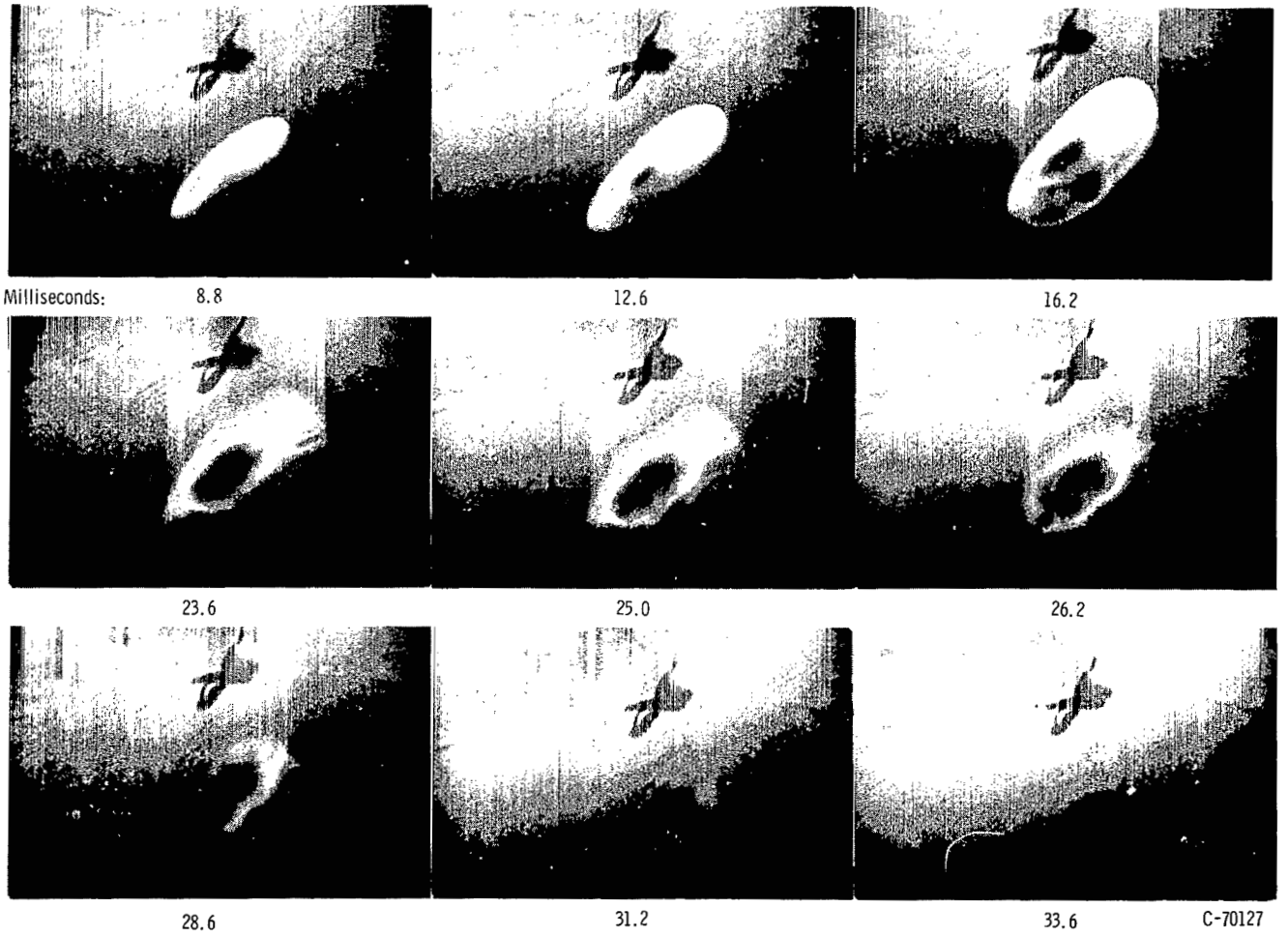

(c) High heat flux.

Figure 7. - Concluded. Observation of microlayer: water boiling on flint glass.

evaporation rate as well as the rate at which latent heat may be drawn from the underlying solid. Drying would be facilitated on a highly conducting metallic surface. It is difficult to predict, however, how the drying phenomenon will be altered at pressures of 1 atmosphere and greater.

Mechanism of bubble release. - Interesting observations of the nature of bubble release can be made from figure 7. At the onset of collapse, the perimeter of the bubble base, which had been sharply demarcated during growth, becomes indistinct; the microlayer apparently becomes thicker at its outer edge and loses definition, much as if surface tension were pulling the bubble into a spherical shape. The bubble lifts quickly away from the surface as long as its base is wetted by a liquid film. In figure 7(c), 7.6 milliseconds are required for release of the wetted 87.5 percent of the bubble base. When a central dry spot is reached, apparently a contact angle opposes the flooding liquid, and the lifting-off process is retarded. The dry 12.5 percent of the bubble base diminishes more gradually and requires 6.2 milliseconds for complete flooding. The boundary of the dry spot is always sharp, indicating that a definite contact angle is formed. In figure 7(b), flooding is similarly retarded at the dry spot. The wetted 93 percent of the base is flooded in 15.8 milliseconds and the dry 7 percent in 10.0 milliseconds.

There is some evidence that the stages of bubble release are instrumental in the formation of vapor columns. Discrete bubble columns have been photographed (ref. 9) and it was noted that, under certain conditions, bubbles depart singly from the surface but only partial flooding occurs.

Pinching-off takes place at the bubble stem so that a small mass of vapor is left in contact with the surface. The photograph in figure 8 (ref. 9) illustrates bubble release at the moment of pinching-off. A new bubble grows immediately from the vapor residue, apparently bypassing the process of nucleation. It is not known at present whether pinching-off occurs generally between discrete bubble columns and vapor columns, or whether it is dependent on a narrow range of boiling conditions. Pinching-off is consistent for successive bubbles at a given site, however. Apparently the surface beneath the residual vapor is dry, indicating that liquid could not flood the surface easily against a contact angle as was seen to be the case in figures 7(b) and (c). When pinching-off occurs in a bubble column, one would expect vapor evolution to be continuous if the residual vapor mass begins to grow before pinching-off is completed. A vapor column formed in this way would have a dry center with a microlayer being formed periodically around the dry spot. Intermittent vapor evolution from the microlayer causes the column perimeter to oscillate near its base,

Figure 8. - Pinching-off phenomenon at bubble base (ref. 9).

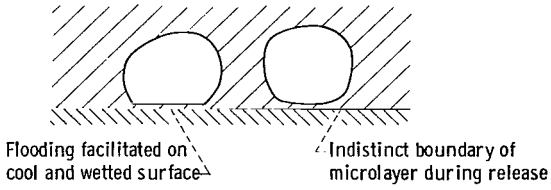

(a) Release of discrete bubbles.

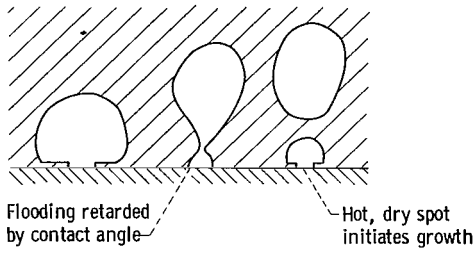

(b) Pinching-off phenomenon.

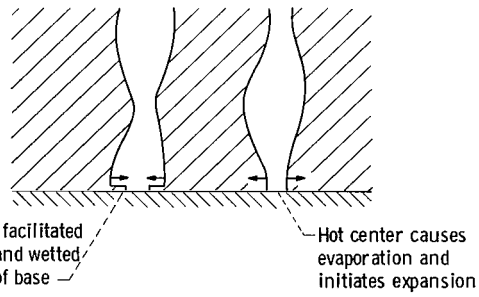

(c) Continuous vapor removal.

Figure 9. - Vapor column formation.

in turn, causing periodic replenishment of the film. This evolution of bubble column to vapor column is shown in figure 9.

Extrapolating observations from a narrow range of conditions is always dangerous, but the model of vapor column formation (fig. 9) could explain two important boiling observations. First, in the vapor column of figure 9(c), evaporation takes place in the vicinity of the wall so that the heat transfer is almost independent of T_b. The insensitivity of the upper regions of the nucleate boiling curve to subcooling is well known (ref. 10, p. 389). Some writers (ref. 11) have postulated that evaporation occurs at the vapor column walls inside the layer of superheated liquid. It seems unlikely that more than a small fraction of the total heat transfer takes place here, since the thickness of the superheated layer depends strongly on subcooling. Second, it has been shown (ref. 1) that the extremely rapid temperature drop associated with surface evaporation occurs cyclically in high heat flux (135,000 to 202,000 Btu/(hr)(sq ft)) nucleate boiling; this experiment demonstrates that the microlayer is an important mechanism of heat transfer in the regime of vapor columns. Furthermore, descriptions of the vapor column in the literature (refs. 11 and 12) agree that complete surface flooding never occurs. If these descriptions are accurate, some kind of oscillation at the column base must be responsible for periodic creation of the microlayer.

Experiment B

A photographic sequence of a microlayer interference pattern is shown in figure 10. Three white and two dark fringes are visible; these fringes increase in diameter as the film evaporates.

In order to be confident of the photographic interpretation, it is necessary to show that the pattern originates from the glass boiling surface and that the rings are actually an interference phenomenon. That the film occurs on the glass boiling surface rather than the plastic window is evident from three considerations. First, the plastic window was not quite parallel to the glass disk so that the reflection was not alined with the camera lens. A

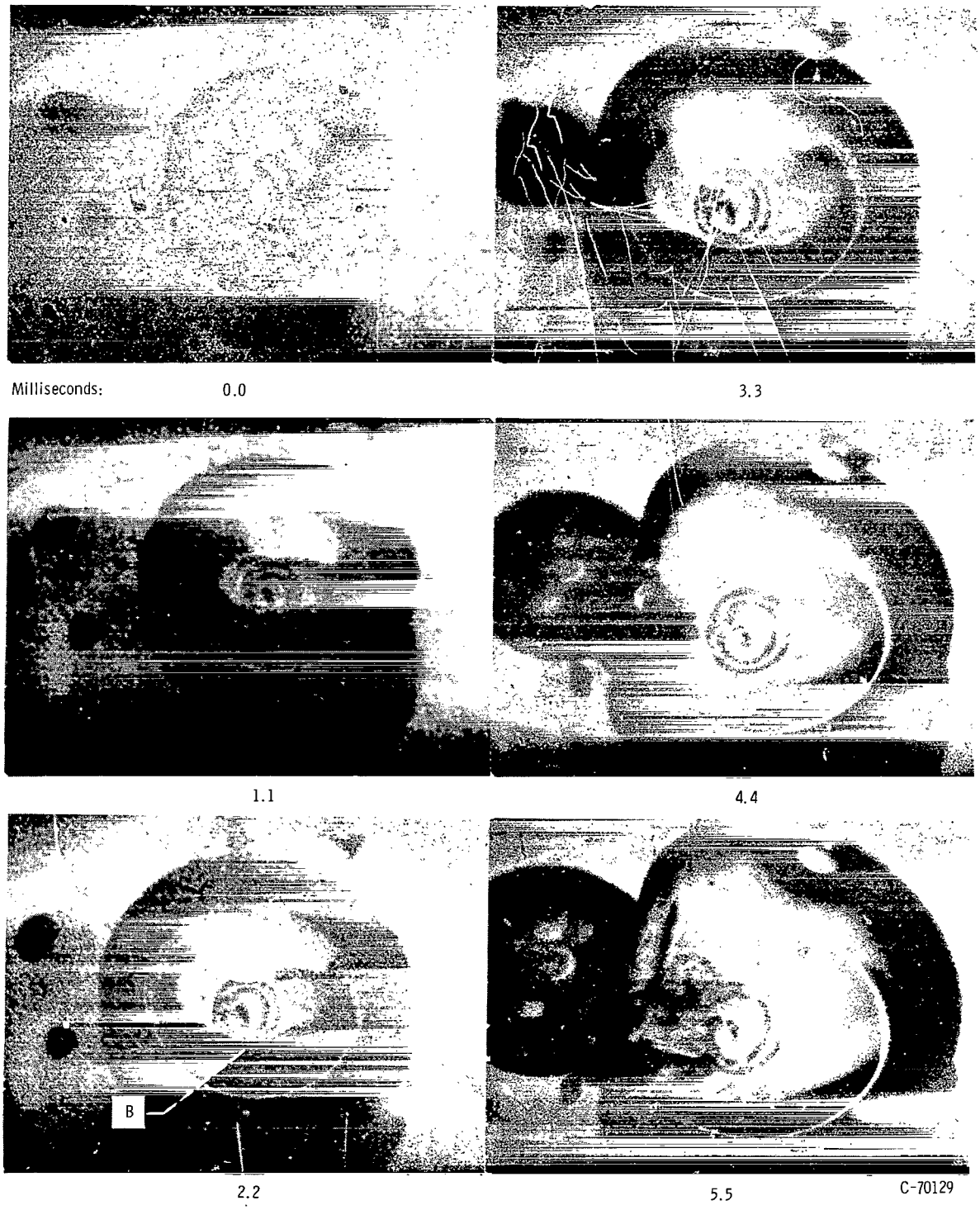

Figure 10. - Microlayer interference pattern: water boiling on flint glass.

scratch, which served as a nucleation site, was used for focusing and assured that the glass rather than the window was in correct alinement. Second, the second and third photographs of figure 10 show that the pattern is partially obscured at B, where the bubble wall meets the plastic window; as the bubble grows larger, the interference pattern is seen in its entirety. This phenomenon could occur only if the film is on the glass boiling surface. And third, since virtually no reflection takes place at the nucleation scratch, the light intensity at the scratch is the upper limit of reflected intensity from the plastic window. The scratch appears almost as dark as interference minimums, and, consequently, the pattern could not be on the window.

Control pictures (fig. 11), viewing a particular bubble simultaneously with white and monochromatic light (fig. 4(b), p. 7), were taken to verify that the observed pattern is caused by an interference phenomenon. The monochromatic view shows two dark rings, A and B, the same number seen in figure 10. In the white view, only a faint central dark ring A' is apparent; this single minimum is to be expected from the mercury line spectrum if one assumes that the center of the pattern is a dry surface. Interference phenomena in the control experiment are discussed in relation to the energy distribution of the mercury spectrum in appendix A.

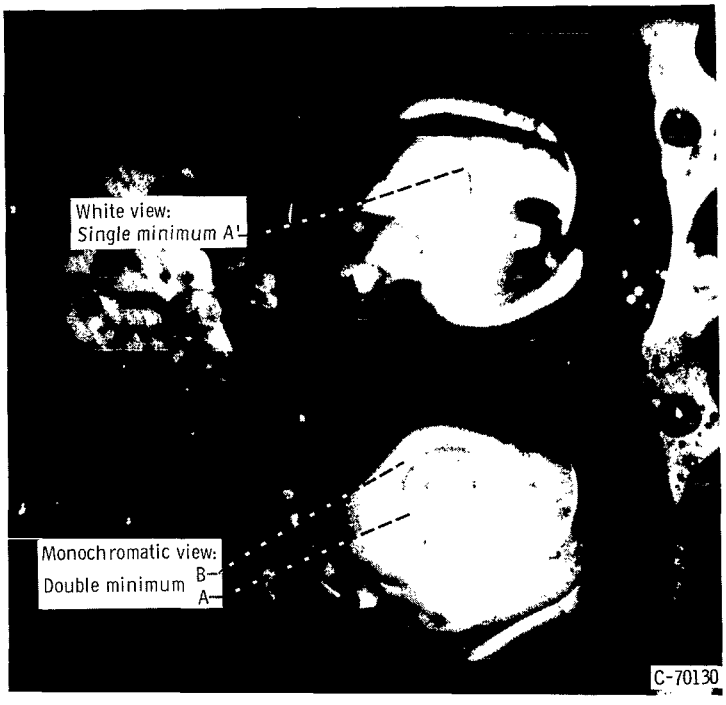

Figure 11. - Simultaneous views of microlayer with white and monochromatic light.

A plot of film thickness profiles against radius for successive intervals of 1.1 milliseconds is shown in figure 12. This plot was made from the photographs of figure 10. By extrapolation of the curves beyond the smallest minimum, it is evident that the center of the film is dry; this result is to be expected from the photographs of experiment A, also taken for the condition of water boiling on flint glass at similar heat flux and pressure. As discussed previously, drying is also indicated by double-beam control experiments.

Local heat fluxes out of the evaporating microlayer have been calculated in appendix B from the data in figure 12. Average values for successive 1.1-millisecond intervals are given in table II; these values refer to an area directly beneath the evaporating film only and are not an average for the entire bubble base. The mean calculated value is 38,000 Btu per hour per square foot. No overall diminution or augmentation with time is observed in the heat flux, and it is difficult to attach significance to the observed cyclic trend. Note

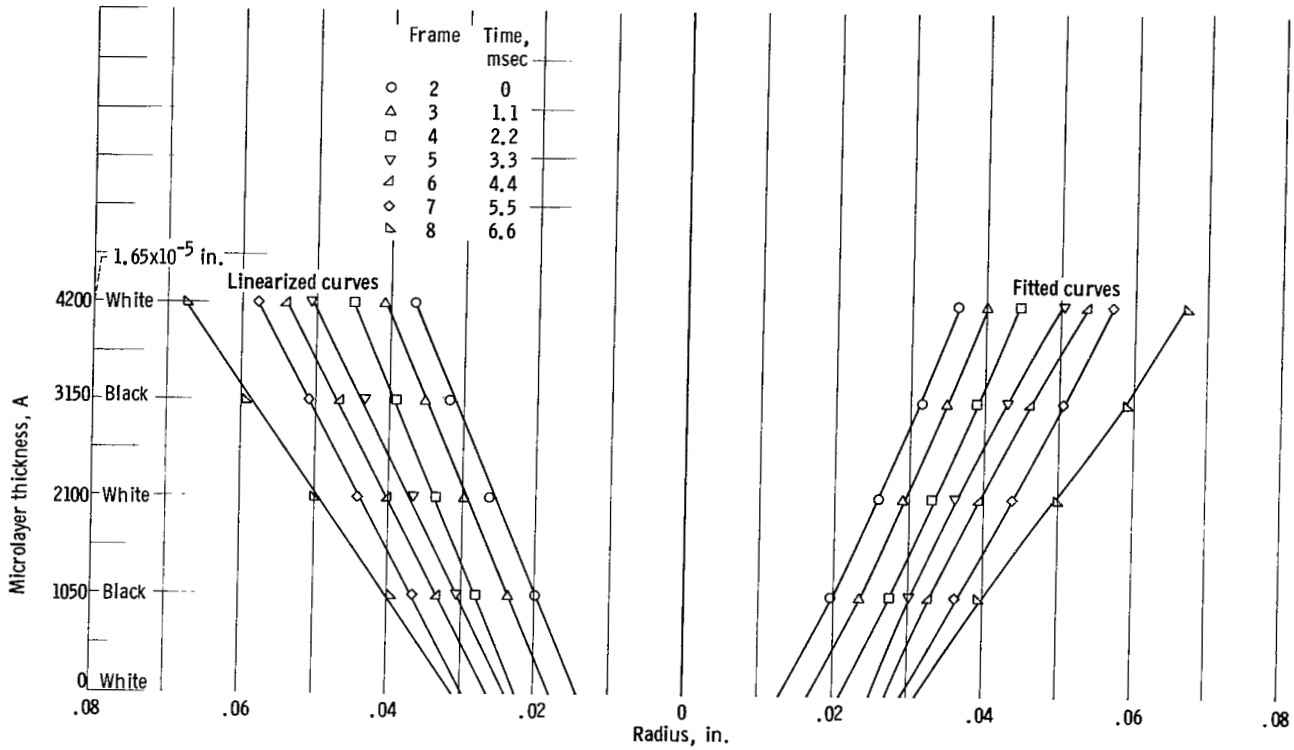

Figure 12. - Microlayer thickness as function of radius.

that the calculated values of heat flux are an order of magnitude less than the values reported in reference 2; the reason for this difference is discussed in the following section.

TABLE II. - HEAT FLUX CALCULATIONS

Frame	Slope of thickness profiles, m	Constant, c, in.	Maximum radius, r_{max}, in.	Average values between successive frames	
				Volume, V, cu in.	Heat flux, q, Btu/(hr)(sq ft)
2	1390	0.014	0.037	11.3×10^{-9}	42,000
3	1390	0.018	0.041	14.7×10^{-9}	50,000
4	1330	0.023	0.045	13.5×10^{-9}	36,000
5	1510	0.025	0.050	12.5×10^{-9}	29,000
6	1630	0.027	0.054	15.5×10^{-9}	32,000
7	1690	0.030	0.058	29.5×10^{-9}	41,000
8	2240	0.031	0.068		

DISCUSSION

Direct (refs. 1, 2, and 4) and indirect (ref. 13) evidence has been presented to show that microlayer evaporation carries most of the heat transfer in moderate and high heat flux nucleate boiling regimes. In view of the importance of an evaporative mechanism, it is useful to consider the system variables that limit the transient heat-transfer process. Primarily, evaporation will be controlled by bubble size, frequency, and population; these variables put an upper limit on the surface area covered by an evaporating microlayer. Secondly, evaporative heat flux will be controlled by the rate-determining variables and by any surface or microlayer condition that causes surface drying or decreases the area available for evaporation. Discussion will be limited to this second group of variables.

Influence of Wall Material

The rate of evaporation from a liquid film is determined at any time by the film superheat ΔT_{sat}. If the liquid film is in contact with a thermal conductor and if the film drops rapidly in temperature as evaporation proceeds, a portion of the necessary latent heat of vaporization will be withdrawn from the thermal capacity of the underlying solid by a transient heat-conduction process. The exact portion depends on the mass and superheat of the film, the steady-state heat flux through the wall, and the thermal characteristics of the wall material. In the case where the heat flow into the film is much greater than the steady-state heat flux and where the film mass or superheat is small, transient conduction from the wall, accompanied by a rapid surface temperature drop, will control local evaporation rates. A water film that evaporates to dryness and carries a superheat of 90° F contains less than 10 percent of its own latent heat; when most of the initial film liquid undergoes evaporation, the film mass may be considered "small."

Transient evaporative heat fluxes have been observed (refs. 1 and 2) and are calculated in appendix B from the data of figure 12. In references 1 and 2, the evaporative fluxes range from six to 20 times the gross surface flux. Average heat-flux measurements could not be taken for the data in table II, but since boiling occurred near the incipience point, it is assumed that the evaporative fluxes ($\approx$40,000 Btu/(hr)(sq ft)) are approximately three times the gross surface flux.

Apparently, evaporation is controlled by a transient conduction process, which is caused by a rapid drop in surface temperature. This condition is approximated by a temperature pulse on a semi-infinite surface; the solution (ref. 14, p. 255) shows that the heat flux out of the solid at a given time after the pulse is proportional to $(k/\sqrt{\alpha})\Delta T$. The microlayer itself is virtually unitemperate; 95 percent of any temperature pulse is transmitted across a water film 10,000 angstroms thick within 0.64 microsecond (see ref. 14, p. 254). The transient evaporative pulses last from 1 to several milliseconds (refs. 1 and 2). Consequently, microlayer evaporation rates on different surfaces at the same instant should vary according to $k\sqrt{\alpha}$ of the material.

A comparison of the transient heat flux data from table II for glass and from reference 2 for Nichrome does substantiate this view of the effect of material. Distilled water, boiling under low pressures of 2 to 3 inches mercury, was used in experiment B and in reference 2.

In both cases, boiling took place well inside the regime of single bubbles near the incipience of the boiling curve. Since the Nichrome surface has a far more extensive distribution of nucleation sites than a polished glass surface, even including the nucleation scratch ΔT_{sat} at incipience for the Nichrome will be equal to or less than ΔT_{sat} for the glass surface. Evaporation from the film will be controlled either by the driving temperature $T_f - T_{sat}$ or by the rate at which heat is supplied to the film from the underlying solid. Since the evaporative fluxes in the case of boiling on glass are less than one-tenth of the values for boiling on Nichrome (38,000 compared with 500,000) even though the ΔT_{sat} is greater for glass, the thermal properties of the wall evidently control the evaporative rates from the film. Quantitatively, the transient heat fluxes for glass and Nichrome should be in approximately the same ratio as the respective values of $k/\sqrt{\alpha}$. The heat fluxes are in the ratio 500,000/38,000 = 13.1, which is near the ratio of $k/\sqrt{\alpha}$, 0.35/0.031 = 11.3 (see table III).

TABLE III. - $k/\sqrt{\alpha}$ FOR VARIOUS BOILING SURFACES

Material	Density, ρ, g/cm^3	Specific heat, c_p, cal/(g)(°C)	Thermal conductivity, k, cal/(cm)(°C)(sec)	$k/\sqrt{\alpha}$, cm^2/sec	Reference
Copper	8.96	0.092	0.94	0.882	15
Nickel	8.9	.105	.22	.455	↓
Platinum	21.5	.032	.17	.342	↓
Chromium	7.19	.11	.16	.357	↓
Flint glass	[a]4.04	.12	.0019	.031	↓
Nichrome	8.4	.107	.134	.346	16
Inconel	8.3	.11	.036	.031	16

[a]Empirically determined.

Whenever microlayer evaporation is inhibited by wall materials of decreasing $k/\sqrt{\alpha}$, a higher wall temperature is required to maintain a constant overall evaporative heat flux. Since the evaporative heat flux has been shown to be a major fraction of the total ebullient heat transfer (refs. 1, 2, 4, and 13), surface materials with decreasing $k/\sqrt{\alpha}$ should have boiling curves displaced to the right; that is, a greater ΔT_{sat} is needed to sustain a given heat flux level. Of the eight metals with three liquids reported, this trend is borne out. In reference 17 boiling curves are shown for plated copper, gold, and chromium with ethanol. Reference 5 shows curves for lapped copper, nickel, and Inconel with pentane, and reference 10 shows curves for polished platinum (2/0 emery) and copper (4/0 emery) with water.

Within each experimenter's data, the surface material of highest $k/\sqrt{\alpha}$ gives the steepest boiling curve (values of $k/\sqrt{\alpha}$ are listed in table III).

It can be argued that different surface materials, given the same degree of polish, will have different active site distributions that could be responsible for the surface effect noted previously. Site distribution increases rapidly with roughness (ref. 18), however. The data of reference 10 show that the nucleate curve for a roughened platinum surface can occur at a higher ΔT than for a polished surface, indicating that the site distribution alone is not sufficient to account for the surface effect.

Thin Wall Effect

During a surge in heat flux under the bubble base, appreciable heat will be withdrawn only from a depth of a few hundredths of an inch beneath the surface. For a temperature pulse of t milliseconds, an appreciable change (greater than 10 percent) of the wall temperature will occur within a depth $d = 2.4\sqrt{\alpha\tau}$ (see ref. 14, p. 254). A pulse of 2-millisecond duration was observed in reference 1 where it was pointed out that most of the heat extraction during the pulse occurs within 0.010 inch of the surface. Presumably, if the boiling surface (ref. 1) were made thinner than 0.010 inch, the transient heat flux would have been limited by the thermal capacity, as well as the thermal properties of the wall. In reference 2 microlayer evaporation was observed on a 0.001-inch-thick ribbon and it was found that the evaporative pulse was strongly limited by the heat content of the ribbon. Apparently, only the thermal properties of the wall within a few hundredths of an inch beneath the surface exert a strong effect on the evaporative flux and the boiling curve. Also, when the heater wall is so thin that it no longer acts as a semi-infinite solid at the bubble base, a restricting effect on the boiling curve (requiring higher ΔT_{sat} for an equivalent q) will be seen. Predicting the thickness at which heater dimensions disturb the transient fluxes is somewhat complicated by the fact that the temperature drop is not instantaneous. Even more difficult is the task of predicting, without specific experimental evidence, exactly where a limitation on transient heat flux, due to wall thickness, causes a change in the boiling curve. One constructive application suggested by wall thickness and material effects is that thin platings of materials with high $k/\sqrt{\alpha}$ could be used to yield greater heat-transfer coefficients and possibly to raise the burnout point as well (ref. 3, p. 20, discussion by Edwards).

Stability of Microlayer

During the boiling of mercury in a glass vessel, one can readily observe that most of the area at the bubble base is swept clear of liquid as the bubble grows. Extensive drying occurs even at the lowest heat fluxes and is apparently caused by the nonwetting surface condition. One cannot determine visually whether a small microlayer is present around the perimeter of the base and if not, where evaporation takes place, but there is no doubt that the nonwetting surface modifies microlayer formation drastically. Partially wetted solids, which are used in most boiling applications, may also cause the microlayer to be unstable resulting in severe limitation of the evaporative heat flux. The author attempted to observe whether or not a stable film could exist

on plastic, but boiling on plastic was impossible without warping the surface. Various investigations of the wetting effect on nucleate boiling have given conflicting results. The most highly controlled experiments performed are reported in reference 19, where different wettabilities were obtained by boiling stearic acid on different faces of a single copper crystal. The data show that the higher contact angle allows a higher heat flux at given ΔT_{sat}. Of course, this experiment covers only one special condition, but it does indicate that a partially wetted surface affects other system variables, perhaps nucleation, more strongly than the tendency of a film to become unstable. The surface temperature profiles of reference 2 also indicate that the liquid film remained stable for several milliseconds on a partially wetted Nichrome surface. It is probable, therefore, that partially wetted metallic surfaces do not interfere seriously with formation of the film. Considering the transient nature of bubble formation and the many variables concerned, it will not be easy to determine under what conditions poor wettability begins to affect microlayer integrity.

SUMMARY OF OBSERVATIONS AND CONCLUSIONS

As the result of the experiments reported herein, a microlayer film at the base of nucleate bubbles has been shown to exist. The continual evaporation from this layer explains the high heat-transfer coefficients associated with nucleate boiling. Furthermore, there seems to be evidence that this microlayer is present in the high heat flux regimes of nucleate boiling when vapor columns are present.

The evaporative heat flux from the microlayer film is dependent upon the material of the heat-transfer surface and seems to vary directly with $k/\sqrt{\alpha}$. In addition, the thinness or amount of material in the heat-transfer surface can affect the evaporative process.

The surface properties of the heat-transfer surface such as finish and wettability will determine the stability of the microlayer. Nonwetting surfaces will tend to destabilize the layer.

Lewis Research Center
National Aeronautics and Space Administration
Cleveland, Ohio, July 22, 1964

APPENDIX A

INTERFERENCE OF MERCURY WHITE LIGHT

Figure 13 shows the absolute energy output of the mercury bulb used (BH-6) for successive 100-angstrom intervals. Flint glass elements in the optical system and the high-speed camera caused rapid attenuation of the ultraviolet between 3400 and 4000 angstroms (information received in a private communication with M. C. Burrows of Lewis). For this reason, the strong blue lines between 4050 and 4400 angstroms, and the green lines (near 5461 A) are considered to contain most of the radiant energy that is passed through to the film. The green line alone (5461 A) contains 35 percent of the spectrum energy. Relative intensities of the two bands can be obtained from figure 13 and are 1.65 and 1.35 for lower and higher wavelengths, respectively. The reflected intensity (in arbitrary units) against film thickness is plotted in figure 14 for both of these wavelengths; the curves, of course, are sinusoidal with minimums at $t = (2l + 1)\lambda / 4n \cos \theta_r$ and with relative amplitudes in proportion to the relative energies. The physical system considered is a water film on a glass surface with $n = 1.77$; for this system, reflection from both interfaces is equal and intensity minimums are zero. Intensity fluctuations, however, have the same dependence on film thickness as for the glass surface used, $n = 1.69$.

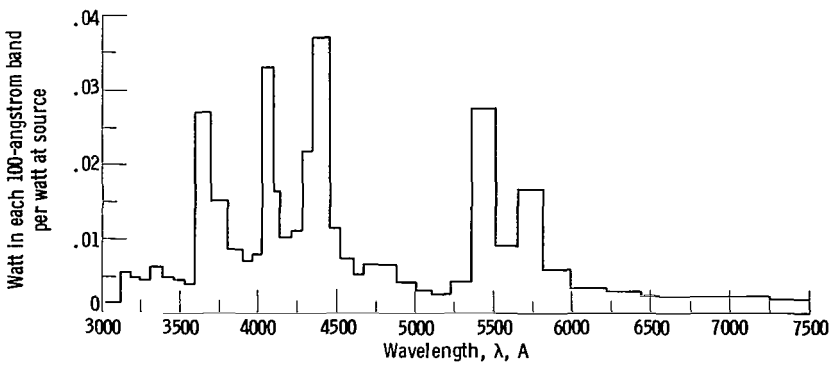

Figure 13. - Energy emission from BH-6 mercury arc lamp (data received from M. C. Burrows of Lewis).

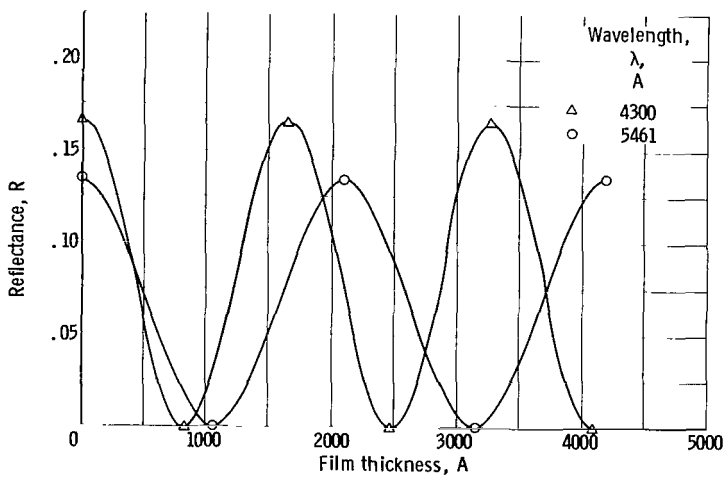

Figure 14. - Reflectance as function of thickness for thin water film.

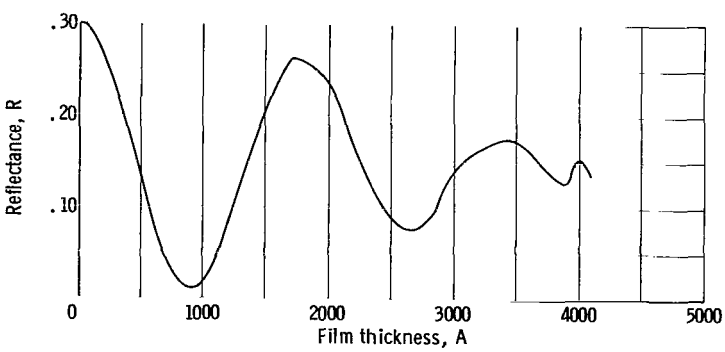

Figure 15. - Resultant reflectance from a water film for two wavelengths plotted in figure 14.

Superimposing the curves in figure 15 gives a first approximation for the reflected intensity of mercury white light as a function of film thickness. It is evident that if the center of the pattern is dry, only the first minimum will be strong, although a very faint dark ring might be seen at $t = 2700$ angstroms. Figure 11 (p. 17) shows simultaneous patterns of the same bubble for white and monochromatic light. The monochromatic view shows two minimums, the same number seen in figure 10 (p. 16). The white view shows only the first minimum, although in certain other photographs, a very faint second minimum was also discernible. The patterns of figure 11 are consistent with an interference phenomenon and also suggest that the central rings, A and A', are unit minimums.

APPENDIX B

HEAT FLUX CALCULATIONS

The data of figure 12 (p. 18) were used to calculate transient evaporative heat fluxes from the microlayer during successive 1.1-millisecond intervals. The circular fringes in figure 9 (p. 15) show that the film is radially symmetric. To determine the volume of liquid evaporated between succeeding frames, the thickness profiles were approximated by straight lines $r = mt + c$, where t is film thickness, r is radius, m is the slope, and c is the radius at which drying occurs. The volume of liquid evaporated between two frames is the conical shell between adjacent profiles. Each shell can be broken up into rings, with thickness dt and area $2\pi r'_t \Delta r_t$; r'_t is the average radius at t:

$$r'_t = \frac{r_2 + r_1}{2} = \frac{1}{2}\left[(m_2 + m_1)t + (c_2 + c_1)\right]$$

and Δr_t is the ring width:

$$\Delta r_t \doteq r_2 - r_1 = (m_2 - m_1)t + (c_2 - c_1)$$

(Subscripts 1 and 2 refer to inner and outer profiles, respectively.) Letting dV be the volume of a ring gives

$$dV = 2\pi r'_t \Delta r_t \, dt$$

or

$$dV = \frac{2\pi}{2}\left[(m_2 + m_1)t + (c_2 + c_1)\right]\left[(m_2 - m_1)t + (c_2 - c_1)\right]dt$$

Collecting terms and integrating yield

$$V = \pi \int_{t=0}^{t=1.65\times10^{-5}\text{ in.}} \left[\left(m_2^2 - m_1^2\right)t^2 + 2(m_2c_2 - m_1c_1)t + \left(c_2^2 - c_1^2\right)\right]dt$$

and

$$V = \pi\left[(m_2 - m_1)^2 \frac{t^3}{3} + (m_2c_2 - m_1c_1)t^2 + \left(c_2^2 - c_1^2\right)t\right]_{t=1.65\times10^{-5}\text{ in.}}$$

The constants m and c were computed from the straight left-hand profiles in figure 12 and are listed in table II (p. 18). Profiles in the right half of the figure are faired to the data points.

Transient heat fluxes are calculated from the liquid volume

$$q = \frac{\rho V H_{vap}}{A \, \Delta\tau}$$

The area A of the microlayer is taken to be $\pi\left(r_{2,max}^2 - c_2^2\right)$ where $r_{2,max}$ refers to the maximum radius of the outer shell profile. Superheat in the film is neglected as an energy source for evaporation since the film evaporates to dryness; even a 90° F superheat supplies less than 10 percent of the heat necessary for total film evaporation. Computed values of the heat flux are listed in table II.

It must be recognized that heat fluxes beneath a newly formed portion of microlayer will be greater than at the point where the film is approaching dryness; in the latter case the film temperature is relatively low. Maximum heat fluxes may, therefore, be higher than computed values in table II.

The calculated heat fluxes have, at best, a two-place accuracy; errors arise chiefly in choosing intensity maximums or minimums on the original photographs and in making straight-line approximations on the profiles. The average value of the evaporative heat flux is 38,400 Btu per hour per square foot, and the average deviation from the mean is 6000 Btu per hour per square foot or 15.6 percent; this latter value provides a conservative estimate of random uncertainties. Systematic error due to the calculational technique is unknown but is probably small compared with random error.

REFERENCES

1. Moore, Franklin D., and Mesler, Russell B.: The Measurement of Rapid Surface Temperature Fluctuations During Nucleate Boiling of Water. A.I.Ch.E. Jour., vol. 7, no. 4, Dec. 1961, pp. 620-624.

2. Hendricks, Robert C., and Sharp, Robert R.: The Initiation of Cooling Due to Bubble Growth on a Heating Surface. Paper Presented at A.I.Ch.E. Meeting, Los Angeles (Calif.), Feb. 4-7, 1962.

3. Bankoff, S. G., Colohan, W. J., Jr., and Bartz, D. R., eds.: Summary of Conference on Bubble Dynamics and Boiling Heat Transfer. Memo. 20-137, Jet Prop. Lab., C.I.T., 1956.

4. Bankoff, S. G., and Mason, J. P.: Heat Transfer from the Surface of a Stream Bubble - Turbulent Subcooled Liquid Stream. A.I.Ch.E. Jour., vol. 8, no. 1, Mar. 1962, pp. 30-33.

5. Berenson, P. J.: Transition Boiling Heat Transfer from a Horizontal Surface. M.I.T. Tech. Report No. 17, Mar. 1, 1960.

6. Born, M., and Wolf, E.: Principles of Optics. Pergamon Press, 1959.

7. Frank, N. H.: Introduction to Electricity and Optics. Second ed., McGraw-Hill Book Co., Inc., 1950.

8. Jenkins, Francis A., and White, Harvey E.: Fundamentals of Physical Optics. Third ed., McGraw-Hill Book Co., Inc., 1957, p. 511.

9. Siegel, R., and Keshock, E. G.: Effects of Reduced Gravity on Nucleate Boiling Bubble Dynamics in Water. Paper Presented at A.I.Ch.E. Meeting, San Juan (Puerto Rico), Sept. 29-Oct. 1, 1963.

10. McAdams, W. H.: Heat Transmission. Third ed., McGraw-Hill Book Co., Inc., 1954.

11. Gaertner, R. F.: Photographic Study of Nucleate Pool Boiling on a Horizontal Surface. Rep. 63-RL-3357C, General Electric Co., June 1963.

12. Moissis, R., and Berenson, P. J.: On Hydrodynamic Transitions in Nucleate Boiling. Paper 62-HT-8, ASME, 1962.

13. Bankoff, S. G.: A Note on Latent Heat Transport in Nucleate Boiling. A.I.Ch.E. Jour., vol. 8, no. 1, Mar. 1962, pp. 63-65.

14. Jakob, M.: Heat Transfer. Vol. I. John Wiley & Sons, Inc., 1949, p. 255.

15. Marks, Lionel S.: Mechanical Engineer's Handbook. Fifth ed., McGraw-Hill Book Co., Inc., 1951.

16. Anon.: Nickel Alloys. Filing Code Ni-9 (Inconel), Mar. 1954; Ni-41 (Nichrome), Apr. 1958. Engineering Alloys Digest, Inc.

17. Bonilla, C. F., and Perry, C. W.: Heat Transmission to Boiling Binary Liquid Mixtures. Trans. A.I.Ch.E., vol. 37, no. 4, Aug. 25, 1941, pp. 685-705.

18. Kurihara, H. M., and Myers, J. E.: The Effects of Superheat and Surface Roughness on Boiling Coefficients. A.I.Ch.E. Jour., vol. 6, no. 1, Mar. 1960, pp. 83-91.

19. Harrison, W. B., and Levine, Z.: Wetting Effects on Boiling Heat Transfer-Copper Stearic Acid System. Paper 57-HT-29, A.I.Ch.E., 1957.

"The aeronautical and space activities of the United States shall be conducted so as to contribute . . . to the expansion of human knowledge of phenomena in the atmosphere and space. The Administration shall provide for the widest practicable and appropriate dissemination of information concerning its activities and the results thereof."

—NATIONAL AERONAUTICS AND SPACE ACT OF 1958

NASA SCIENTIFIC AND TECHNICAL PUBLICATIONS

TECHNICAL REPORTS: Scientific and technical information considered important, complete, and a lasting contribution to existing knowledge.

TECHNICAL NOTES: Information less broad in scope but nevertheless of importance as a contribution to existing knowledge.

TECHNICAL MEMORANDUMS: Information receiving limited distribution because of preliminary data, security classification, or other reasons.

CONTRACTOR REPORTS: Technical information generated in connection with a NASA contract or grant and released under NASA auspices.

TECHNICAL TRANSLATIONS: Information published in a foreign language considered to merit NASA distribution in English.

TECHNICAL REPRINTS: Information derived from NASA activities and initially published in the form of journal articles.

SPECIAL PUBLICATIONS: Information derived from or of value to NASA activities but not necessarily reporting the results of individual NASA-programmed scientific efforts. Publications include conference proceedings, monographs, data compilations, handbooks, sourcebooks, and special bibliographies.

Details on the availability of these publications may be obtained from:

SCIENTIFIC AND TECHNICAL INFORMATION DIVISION

NATIONAL AERONAUTICS AND SPACE ADMINISTRATION

Washington, D.C. 20546